

The Transition between Nonorthogonal Polarization Modes in PSR B2016+28 at 1404 MHz

Mark M. McKinnon

National Radio Astronomy Observatory¹, Socorro, NM 87801 USA

mmckinno@nrao.edu

ABSTRACT

Polarization observations of the radio emission from PSR B2016+28 at 1404 MHz reveal properties that are consistent with two, very different, interpretations of the pulsar’s viewing geometry. The pulsar’s average polarization properties show a rapid change in position angle (PA) near the pulse center, suggesting that the observer’s sightline nearly intersects the star’s magnetic pole. But single pulse, polarization observations of the pulsar show nearly orthogonal modes of polarization following relatively flat and parallel PA trajectories across the pulse, suggesting that the sightline is far from the pole. Additionally, PA histograms reveal a “modal connecting bridge”, of unknown origin, joining the modal PA trajectories over much of the pulse and following the rapid PA change shown in the average data. The nonorthogonality of polarization modes is incorporated in a statistical model of radio polarization to account for the deviations from mode orthogonality that are observed in the pulsar. The model is used to interpret the rapid PA change and modal connecting bridge as a longitudinally-resolved transition between modes of nonorthogonal polarization. Thus, the modal PA trajectories are argued to reflect the pulsar’s true viewing geometry. This interpretation is consistent with the pulsar’s morphological classification, preserves the Radhakrishnan & Cooke model of pulsar radio emission, and avoids the complication that the modal connecting bridge might be produced by some other emission mechanism. The statistical model’s ability to simulate the rich variety of polarization properties observed in the emission lends additional support to the model’s applicability and its underlying assumption that the polarization modes occur simultaneously.

Subject headings: polarization — pulsars: general — pulsars: individual (PSR B0950+08, B1929+10, B2016+28, B2020+28)

¹The National Radio Astronomy Observatory is a facility of the National Science Foundation operated under cooperative agreement by Associated Universities, Inc.

1. INTRODUCTION

All modern polar cap theories of pulsar radio emission are based upon the hypothesis of Radhakrishnan & Cooke (1969, hereafter RC) that the emission arises from charged particles streaming along open magnetic field lines above the pulsar’s polar cap. The observed polarization due to this particle motion is the instantaneous projection of the magnetic field lines in the emission region on the plane of the sky. If the magnetic field structure is dipolar, the position angle (PA) of the resulting linear polarization vector varies in an S-shaped pattern with pulse longitude as the pulsar’s rotation alters the field-line projection with respect to an observer’s sightline. Since the polarization vector’s orientation is determined solely by the dipolar field structure and the viewing geometry, the observed PAs are essentially frequency-independent. The astonishing ability of the RC model to explain both the PA patterns and the large fractional linear polarization that are actually observed is a testament to the model’s success and popularity for over three decades.

The 1404-MHz polarization observations of individual pulses from PSR B2016+28 by Stinebring et al. (1984, hereafter SCRWB) offer two very different interpretations of the pulsars’ viewing geometry, thereby challenging the validity of the RC model (SCRWB). The longitude-dependent PA histograms presented by SCRWB reveal two, nearly flat, PA traces separated by about 90° across most of the pulse with a connecting bridge between the traces near the pulse center. The two PA traces most certainly arise from the well-known orthogonal modes of polarization (e.g. Manchester, Taylor, & Huguenin 1975, hereafter MTH; Backer, Rankin, & Campbell 1976, hereafter BRC; Cordes, Rankin, & Backer 1978; Backer & Rankin 1980, hereafter BR; SCRWB), and their flat trajectories suggest a viewing geometry where the observer’s sightline makes a large angle with respect to the star’s magnetic pole. But when the SCRWB data are averaged over many rotations of the star, the resulting PAs vary in the classic S-shaped pattern with a steep slope near the pulse center (Fig. 1), suggesting that the sightline nearly intersects the magnetic pole. The steep PA sweep observed in the averaged data is embedded in the modal connecting bridge shown in the single pulse data. The rapid PA change and modal connecting bridge are not apparent in the 430-MHz polarization observations reported by BRC, as one might expect from the frequency independence of the RC model. The PAs of PSR B2016+28 observed at 1404 MHz then pose a multi-faceted dilemma. If the RC model is to be preserved, one must decide which viewing geometry is correct while also developing an explanation for the PA trace that is not attributed to geometry. Furthermore, one must determine the origin of the modal connecting bridge. Is it an artifact of polarization mode interaction or could it be an indicator of another emission mechanism operative in the pulsar magnetosphere?

Despite the conflicting interpretations generated by the 1404-MHz PAs of PSR B2016+28,

its viewing geometry has generally been accepted on the basis of the frequency dependence of its pulse shape. Rankin (1983, 1986, 1993) developed a morphological classification scheme that is based primarily on the spectral evolution of pulse shapes. She categorizes PSR B2016+28 within a group of pulsars designated as “conal single” or “type-Sd” pulsars. The pulse shape of a conal single pulsar evolves from a single component at high frequency to two components at low frequency. This frequency dependence of the pulse shape is thought to result from a combination of the spreading or radius-to-frequency mapping of the conal emission and a tangential traverse of an observer’s sightline across the pulsar’s emission cone. The viewing geometry for conal single pulsars thus requires a large angle between the magnetic pole and the sightline, just as the modal PA trajectories in PSR B2016+28 suggest. The pulsar displays other key characteristics of conal single pulsars (Rankin 1983; Rankin & Ramachandran 2003), such as drifting subpulses and low linear polarization across its entire pulse owing to orthogonally polarized modes (OPM). Hankins & Rickett (1986) investigated the frequency dependence of the average profiles for many pulsars. Specifically recognizing the conflicting interpretations of the 1404-MHz PAs in PSR B2016+28, they noted that the modal PA trajectories in the pulsar are more consistent with the frequency dependence of its profile. Hankins et al. (1992) interpret the 1404-MHz PAs, and thus the pulsar’s viewing geometry, in a similar way. However, no one has adequately resolved the dilemma over the conflicting interpretations of the 1404-MHz PAs or reconciled, in detail, the 1404-MHz PAs with the viewing geometry implied by its morphological classification. Additionally, no one has offered a detailed explanation for the pulsar’s modal connecting bridge.

SCRWB suggested that the modal connecting bridge in PSR B2016+28 and, more generally, the nonorthogonality of the polarization modes may be related to the “migration” of OPM. This mode migration may be the frequency-dependent relocation, spreading, or splitting of modal radiation with pulse longitude. SCRWB also emphasized the need to clarify the nature and importance of nonorthogonal polarization modes (NPM) in the emission. While the occurrence of NPM has been frequently observed and widely documented in the literature (e.g. BR; SCRWB), theoretical investigations (e.g. Cheng & Ruderman 1979; Allen & Melrose 1982; Barnard & Arons 1986; Michel 1987; Gangadhara 1997) and statistical modeling (e.g. McKinnon & Stinebring 1998, 2000; McKinnon 2002) of the modes have concentrated on their orthogonality, but have largely ignored their observed nonorthogonality.

The first objective of this paper is to resolve the dilemma over the conflicting interpretations of the pulsar’s 1404-MHz PAs. I follow the suggestion of SCRWB and argue that the rapid change in average PA along with the modal connecting bridge in PSR B2016+28 is a longitudinally-resolved transition between NPM. In other words, the bridge is simply an artifact of NPM superposition, and not an indicator of another emission mechanism. The second objective of the paper is to account for nonorthogonal polarization modes in a

statistical model of the radio emission’s polarization. In §2, I review the observed polarization properties of PSR B2016+28 by replicating the results of SCRWB, and argue that the modal PA trajectories reflect the true viewing geometry of the pulsar. I incorporate the mode nonorthogonality in a statistical model of superposed OPM (McKinnon & Stinebring 1998, hereafter MS1) in §3. I then describe the predicted effects of superposed NPM on polarization data and compare the predictions with observations. In §4, I discuss the implications of this investigation for radiative processes in pulsar magnetospheres.

2. OBSERVED POSITION ANGLES IN PSR B2016+28

As a point of reference for the discussion in § 3, the observational results of SCRWB are replicated in Figure 1, which shows the average pulse profile of PSR B2016+28 at 1404 MHz. The single pulse, polarization data used to construct the profile were recorded by SCRWB with the 305-m Arecibo radio telescope. The solid line in the bottom panel of the figure shows how the average PA varies across the pulse. The PAs of the pulsar’s nearly-orthogonal polarization modes at each pulse longitude are shown by the triangles in the PA plot, and were estimated as follows.

A PA histogram, similar to those shown in Figure 5, was computed at each pulse longitude of PSR B2016+28 using the single pulse, polarization observations of SCRWB. Each histogram contained 50 equally-spaced bins over the 180° range in possible PA values, giving a histogram bin resolution of 3.6°. Only data samples having a linear polarization that exceeded the off-pulse noise by a factor of five were used to construct the histograms. The PA of the most frequently occurring, or dominant, polarization mode was found by locating the peak in the histogram, and using the peak bin along with 12 bins on either side of it to calculate a weighted mean angle, $\langle\psi\rangle$. From the statistics of directional data described in Mardia (1972), the weighted mean angle was found using

$$C = \frac{1}{N} \sum_{i=1}^{25} f_i \cos(2\psi_i), \quad (1)$$

$$S = \frac{1}{N} \sum_{i=1}^{25} f_i \sin(2\psi_i), \quad (2)$$

$$\langle\psi\rangle = \frac{1}{2} \arctan\left(\frac{S}{C}\right), \quad (3)$$

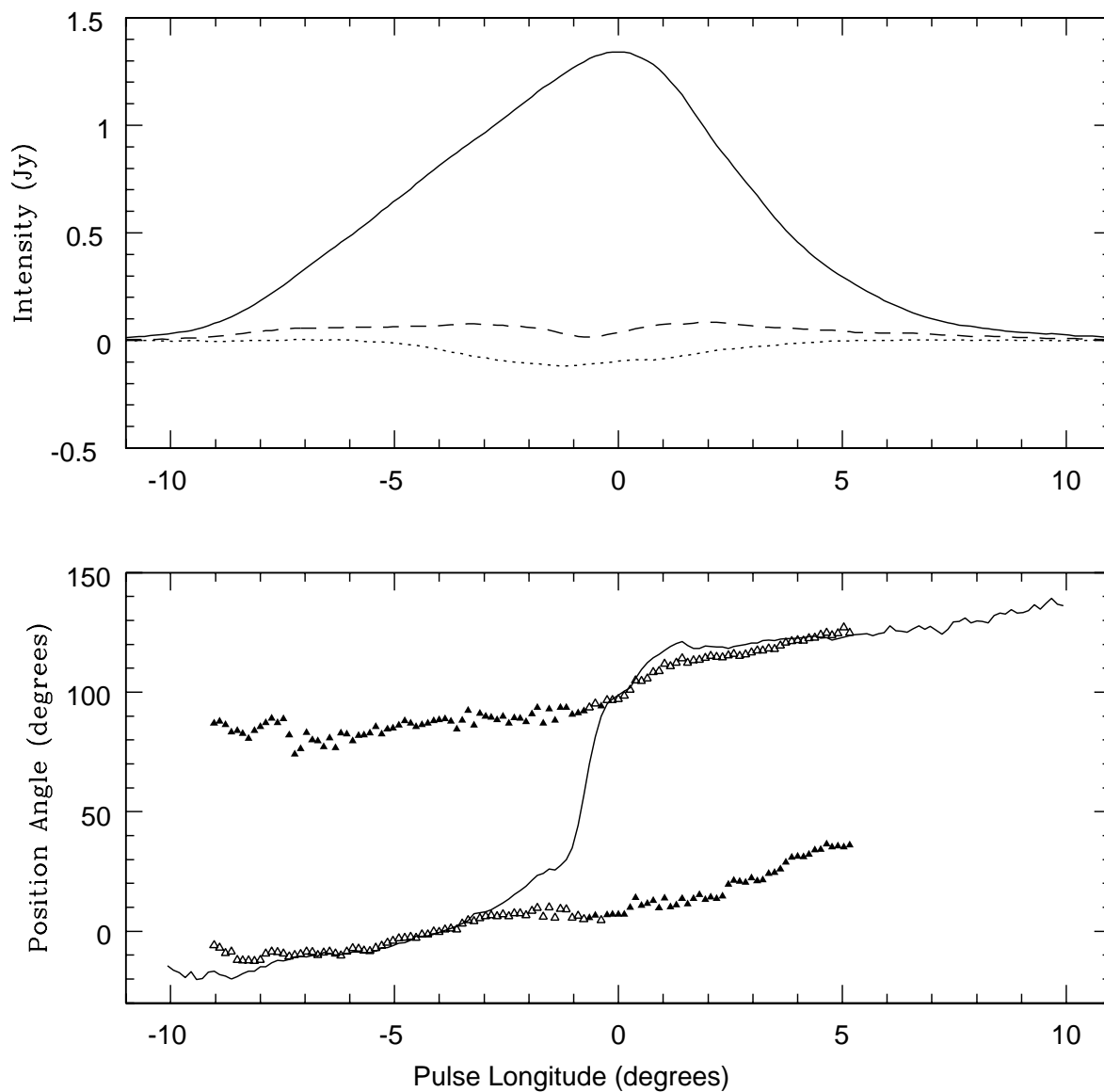


Fig. 1.— Average pulse profile of PSR B2016+28 at 1404 MHz. The total intensity, linear polarization, and circular polarization of the pulse are denoted by the solid, dashed, and dotted lines, respectively, in the top panel. The polarization position angle (PA) determined from the average values of the Stokes parameters Q and U is shown by the solid line in the bottom panel. The triangles in the PA plot denote the peaks in PA histograms constructed from single pulse polarization observations. Open triangles represent the dominant polarization mode, and filled triangles represent the weak mode.

where ψ_i is the midpoint of the PA bin, f_i is the number of data samples in the bin, and $N = \sum f_i$ is the total number of data samples in the 25 PA bins. The open triangles in Figure 1 show the weighted mean angles for the dominant mode at each pulse longitude. The remaining 25 bins in the PA histogram were used to calculate the mean angle of the weak polarization mode (filled triangles in the figure) with the same equations. The resulting PA trajectories of the polarization modes are very similar to those reported in the original observations (see Fig. 31 of SCRWB).

Of the 2700 pulses recorded in the observation, the number of data samples exceeding the detection threshold on linear polarization was as high as 1250, depending on pulse longitude. Data points are not shown in the bottom panel of Figure 1 for any pulse longitude having less than 100 samples in its PA histogram. These locations occur at the pulse edges where the instantaneous signal-to-noise ratio (S/N) in linear polarization is low. Formal errors in $\langle\psi\rangle$ are estimated to range from 6° to 13° , and have been omitted from the figure for clarity.

The primary advantage of calculating modal PAs from equations 1, 2, and 3 is to bring to bear the full weight of the data in making quantitative estimates of modal PAs and their differences, thus helping to identify any deviations from mode orthogonality. A minor disadvantage of this particular method is to introduce a slight bias that skews the difference in modal PAs towards 90° when the PA is nearly uniformly distributed and the linear polarization is very low (e.g. on the pulse edges and near a pulse longitude of -1° in Fig. 1).

The PAs in the bottom panel of Figure 1 clearly illustrate the two interpretations that could be made of the pulsar’s viewing geometry. The average angle changes rapidly with pulse longitude near the pulse center, and its total excursion across the pulse approaches 180° . Both properties are indicative of a viewing geometry where the observer’s sightline passes near the star’s magnetic pole. The trajectories followed by the polarization modes, however, are relatively flat with a total excursion in PA of something much less than 180° , indicating that the observer’s sightline is far from the magnetic pole.

Many features of Figure 1 suggest that the flat PA trajectories of the polarization modes reflect the pulsar’s true viewing geometry. The average PA generally follows the dominant polarization mode (open triangles in Fig. 1) as one would expect from OPM superimposed upon a flat PA trajectory (BRC; SCRWB; MS1). One polarization mode dominates the leading edge of the pulse, while the other dominates the trailing edge. Assuming that the modes occur simultaneously (MS1; McKinnon & Stinebring 2000, hereafter MS2), the low average linear polarization and the frequent occurrence of both modes across the entire pulse imply that the modes have comparable polarized intensities on average (see, also, Rankin 1983; Rankin & Ramachandran 2003). Additionally, the rapid change in average angle near

the pulse center isn't quite as smooth as one would typically expect from the RC model. The rapid PA change joins the modal PA trajectories, and its magnitude is approximately 90° , suggesting that the PA change is related to an OPM transition.

Additional features of Figure 1 suggest that NPM may be complicating our interpretation of the PA pattern in PSR B2016+28. The differences between the modal PAs are almost, but not precisely, 90° across most of the pulse. The mode nonorthogonality does not appear to vary greatly or rapidly across the pulse. While the change in the average angle at the pulse center is rapid, it is not discontinuous as would be expected for a purely orthogonal transition, and so may indicate the presence of NPM (Cheng & Ruderman 1979; SCRWB; Michel 1987).

3. STATISTICAL MODEL OF NONORTHOGONAL MODES

A statistical model for the polarization of pulsar radio emission was presented in MS1 and further developed in MS2 and McKinnon (2002). The model is based upon the observation that the highly polarized, orthogonal modes occur simultaneously. To incorporate the nonorthogonality of the modes in the model, the analysis which follows concentrates on the emission's linear polarization and neglects its circular polarization because NPM are most evident in the observed PA of the linear polarization vector and the circular polarization generally tends to be a small part of the emission's polarization.

As in MS1, let X_1 and X_2 be random variables representing the linearly polarized intensities of the primary and secondary polarization modes, respectively. Without loss of generality, the PA of the primary mode can be set to 0° , which means that the polarization vector of the primary mode points in the direction of increasing Stokes parameter Q in the Q-U plane of the Poincaré sphere (Fig. 2). The polarization vector of the secondary mode generally points in the direction opposite that of the primary mode vector, but makes an angle θ with respect to the Q-axis to account for the nonorthogonality (see Fig. 2). If X_N is a random variable representing the instrumental noise, the observed Stokes parameters Q and U of the combined emission at an arbitrary pulse longitude are

$$Q = X_1 - X_2 \cos \theta + X_{N,Q}, \quad (4)$$

$$U = X_2 \sin \theta + X_{N,U}. \quad (5)$$

Assuming that θ is constant and thus independent of X_2 , the PA calculated from the average values of Q and U is

$$\psi = \frac{1}{2} \arctan\left(\frac{\langle U \rangle}{\langle Q \rangle}\right) = \frac{1}{2} \arctan\left(\frac{\sin \theta}{M - \cos \theta}\right), \quad (6)$$

where $M = \mu_1/\mu_2$ is the ratio of the mean values of the modes' polarized intensities, $\mu_1 = \langle X_1 \rangle$ and $\mu_2 = \langle X_2 \rangle$. Equation 6 shows that the average PA resulting from the superposition of NPM produces an angle intermediate to the PAs of the two modes. For example, when $M = 1$ and the nonorthogonal modes have PAs of 0° and 85° , the deviation from orthogonality is $\theta = 10^\circ$ and the average angle is $\psi = 42.5^\circ$, which is equidistant from the orientations of the two modes.

If the modes are truly orthogonal ($\theta = 0$), the vectors representing their linear polarization are antiparallel in the Q-U plane. The polarization vector resulting from the superposition of OPM is aligned with the PA of the mode having the larger polarized intensity (Fig. 2, example 1). The MS1 statistical model attributes the observed switching between modes to the random fluctuations in their polarized intensities. Within the context of the model, the only way to produce PAs intermediate to those of the orthogonal modes is through the influence of the instrumental noise. PA histograms produced by this model generally contain two peaks, symmetric about their centroids and separated by 90° , with a uniform plateau arising from the instrumental noise (see Fig. 2 of MS1).

When the modes are not orthogonal, their polarization vectors are not antiparallel in the Q-U plane. As can be seen in examples 2 through 4 of Figure 2, the orientation of the vector resulting from NPM superposition is intermediate to the orientations of the mode vectors, and depends upon the modes' polarized intensities and the degree of nonorthogonality (θ in Fig. 2). Also, the superposition of NPM depolarizes the observed emission (i.e. the amplitude of the resultant polarization vector is less than that of the polarization vector for the dominant mode), but not nearly as efficiently as the superposition of OPM.

These signatures of the superposed NPM model should be evident in PA histograms and in the joint probability density, or scatter plots, of PA and linear polarization (L). The PA histograms should be similar to Figure 3, which was constructed from a numerical simulation of equations 4 and 5. The separation of the peaks in the histogram is less than 90° because the modes are not orthogonal. Since PAs intermediate to the orientations of the mode vectors can result from the superposition of NPM, an overabundance of data samples occurs between the peaks, and a paucity of data points occurs outside them. The intermediate values of the resultant PAs also lead to slight asymmetries in the peaks about their centroids. For the L-PA scatter plots, the NPM model predicts that data samples with significant L should occur between the mode peaks.

Figure 4 shows L-PA scatter plots for four pulsars observed by SCRWB. In each plot, the dominant polarization mode is located where the concentration of data points is greatest. The observed Stokes parameters Q and U of each data point have been rotated so that the dominant mode occurs at a PA of $\psi = -45^\circ$ for each pulsar. As predicted by the superposed

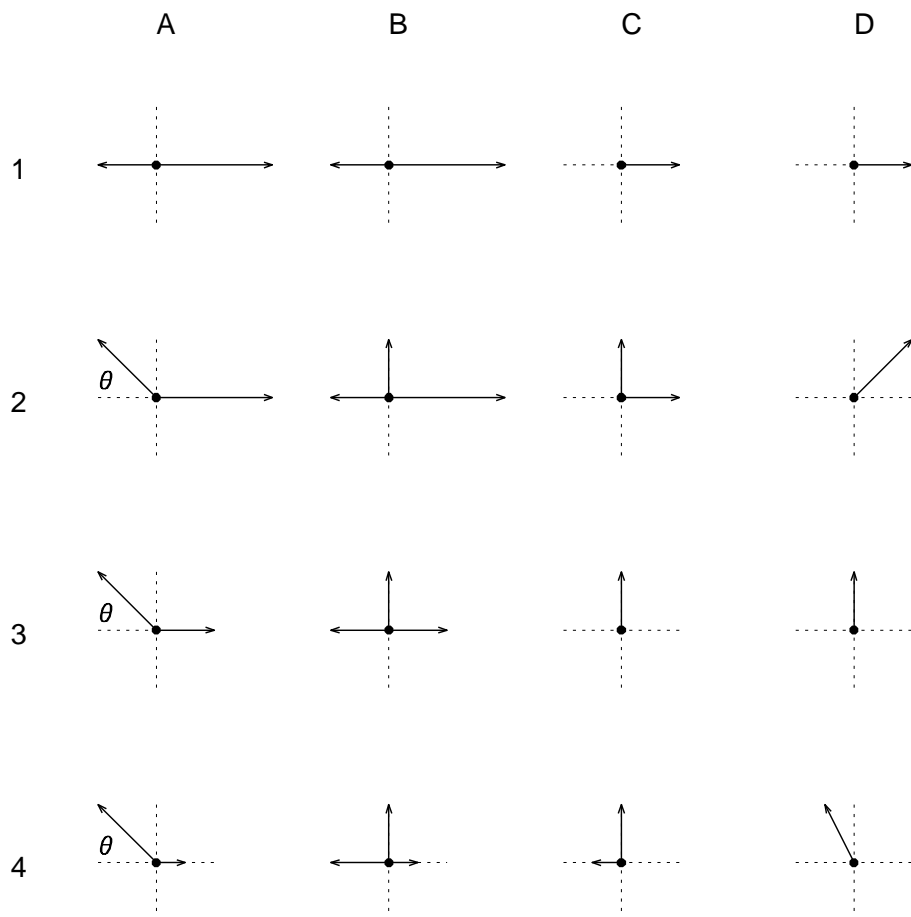


Fig. 2.— Four examples (1-4) of the polarization vector resulting from the superposition of two polarization modes. In each example, column A shows the vectors representing the linear polarizations of the primary and secondary modes. The primary mode vector points to the right in each grid of column A, and the secondary mode vector points towards the left, generally making an angle θ with the horizontal. Column B shows the primary mode and the decomposition of the secondary mode into its orthogonal components. Column C shows the vector sums of the orthogonal components. The resultant vector is shown in column D. The modes are orthogonal in example 1. Examples 2 through 4 illustrate the effect of decreasing the amplitude of the primary mode when the modes are not orthogonal.

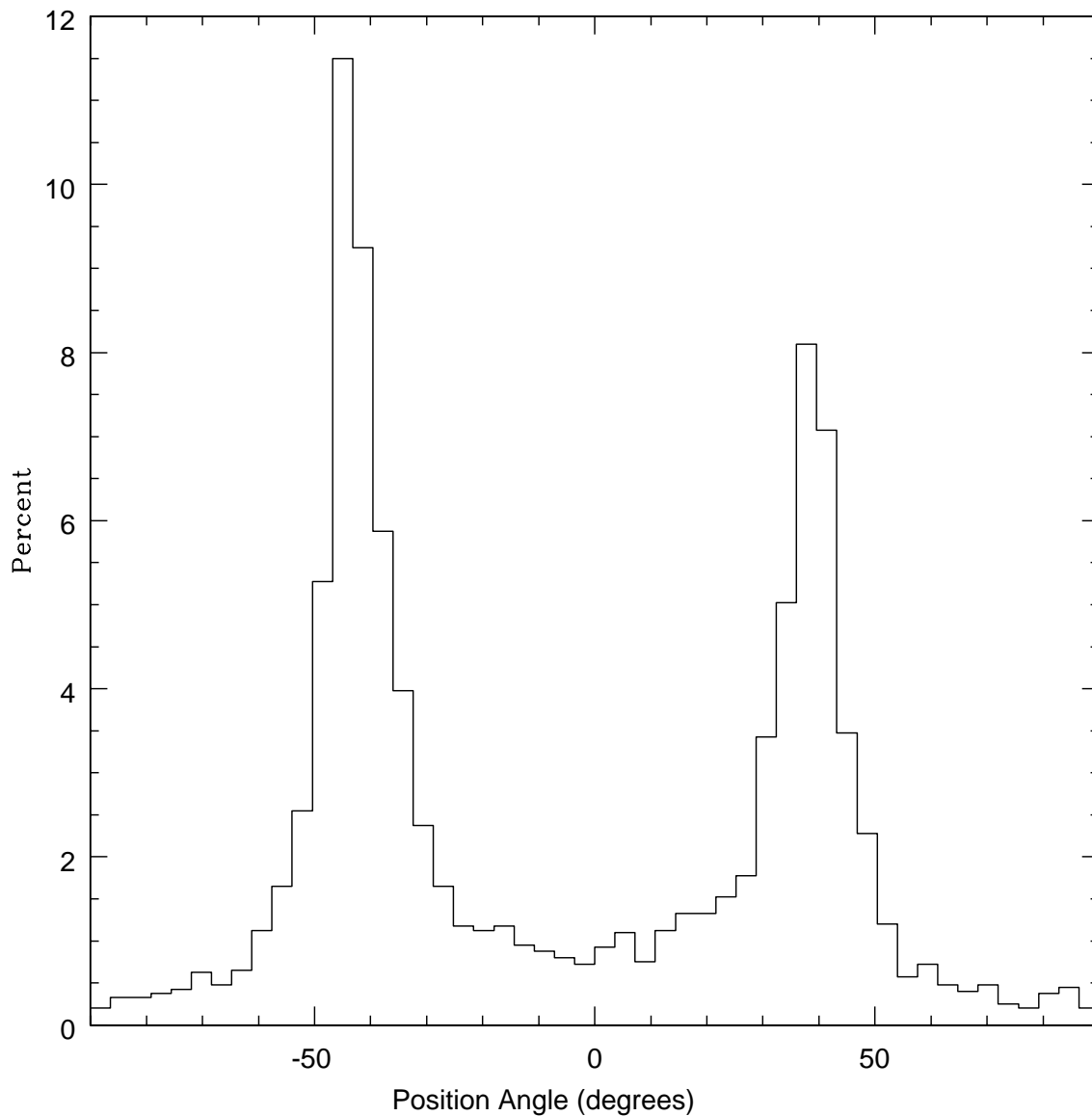


Fig. 3.— Position angle histogram constructed from a numerical simulation of superposed, nonorthogonal modes. The histogram illustrates the characteristics expected from the superposition of nonorthogonal modes (see the text). The mode polarizations were modeled as exponential random variables, and instrumental noise was included in the simulation. The degree of nonorthogonality for the secondary mode was $\theta = 10^\circ$ in the simulation. The peak of the primary polarization mode has been set to -45° for display purposes.

NPM model, many data samples with highly significant linear polarization ($L > 5\sigma_N$) are located between the mode peaks ($-45^\circ < \psi < 45^\circ$). This is particularly true of PSR B0950+08 and PSR B1929+10 where the modes are clearly defined. The modes are not as well defined in the scatter plots for PSR B2016+28 and PSR B2020+28 because the modes occur with similar frequency. As discussed in MS1, this implies the mode polarization amplitudes are similar on average (i.e. $M \simeq 1$), so that their simultaneous interaction leads to significant depolarization of the intrinsic radiation and causes the observed polarization to be dominated by the randomly polarized, on-pulse, instrumental noise (the broad pedestal in the scatter plots).

Figure 5 shows the PA histograms constructed from the scatter plots in Figure 4. As mentioned in § 2, only data points with a S/N in L greater than five (the dashed horizontal line in each plot of Fig. 4) were used to construct the histograms. The separation between the two peaks in each histogram is less than 90° , and of the four examples shown in the figure, the deviation from mode orthogonality is greatest for PSR B2016+28. The four histograms show other similarities in addition to the nonorthogonality of the modes. In each histogram, more data points fall between the peaks than outside them, and the individual peaks are slightly asymmetric about their centroids. The PA histograms bear a remarkable resemblance to the histogram generated with the numerical simulation of the superposed NPM model (Fig. 3).

Turning now to the PA calculated from the averaged Stokes parameters, consider a hypothetical situation where one had *a priori* knowledge of a pulsar’s viewing geometry. This being the case and barring the limitations of S/N, one could easily remove the systematic effect of the RC PA sweep from the data. Having done this, the variation in PA across the pulse attributable to the polarization modes would be described by equation 6, where M and θ are now dependent on pulse longitude. The primary mode would occur at pulse longitudes having $M > \cos\theta$, the secondary mode would occur at longitudes with $M < \cos\theta$, and a mode transition would occur at longitudes where $M = \cos\theta$. If the deviation from orthogonality is small and constant ($\theta = \theta_o \ll 1$) over the range of pulse longitude where the mode transition occurs and if the modal ratio, M , varies linearly with longitude (e.g. $M(\phi) = 1 + a(\phi - \phi_o)$) over the same range, the rate the PA changes with pulse longitude near the mode transition is

$$\frac{d\psi}{d\phi} \simeq -\frac{a}{2\theta_o}. \quad (7)$$

Equation 7 shows that the mode transition is abrupt when the modes are orthogonal ($\theta_o = 0$), but gradual when the modes are not orthogonal ($\theta_o \neq 0$). The equation also suggests that

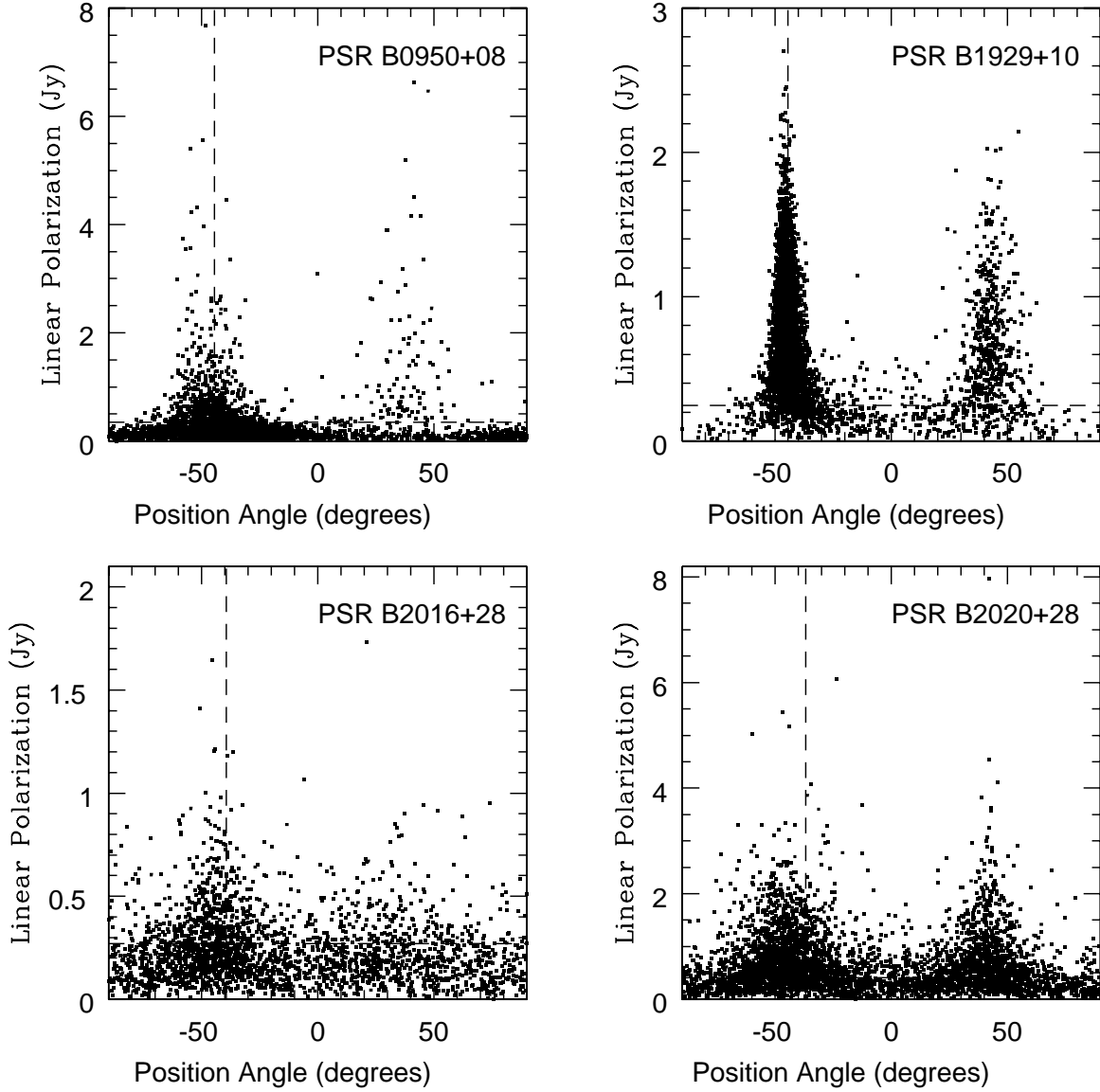


Fig. 4.— Scatter plots of position angle (PA) and linear polarization (L) at a single pulse longitude in each of PSR B0950+08, PSR B1929+10, PSR B2016+28, and PSR B2020+28. The dashed horizontal line in each plot is drawn at a power level corresponding to five times the off-pulse noise. Many data samples with significant L, particularly in PSR B0950+08 and PSR B1929+10, are located between the mode peaks as predicted by the NPM statistical model. The vertical line denotes the location of the PA computed from the average values of Stokes Q and U. For display purposes, the original values of Q and U were rotated so that the PA of the dominant polarization mode occurs at -45° .

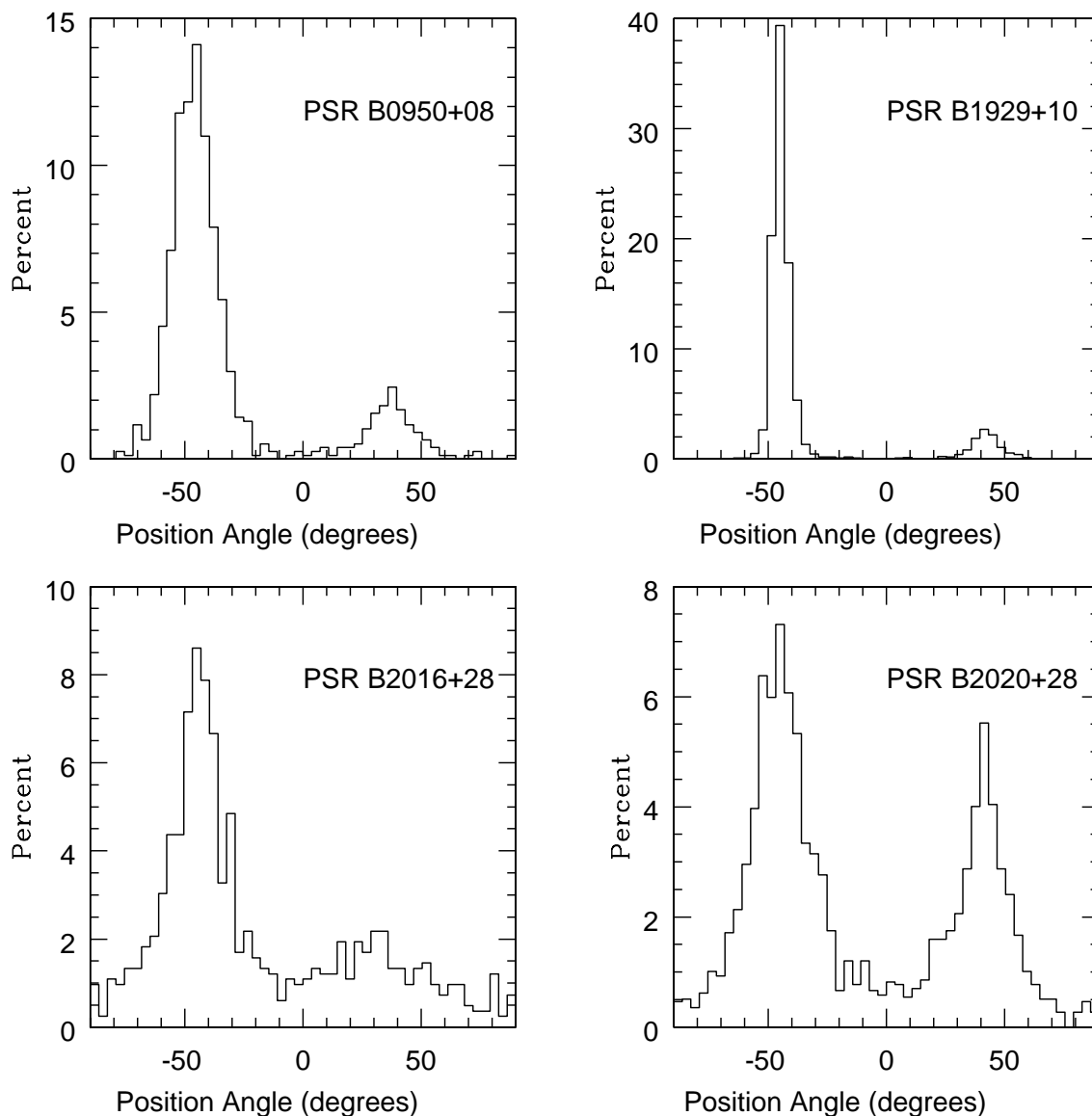


Fig. 5.— Position angle (PA) histograms constructed from the scatter plots in Fig. 4. In each case, the separation in histogram peaks is less than 90° , indicating that the polarization modes in each pulsar are not orthogonal. The peak of each histogram, which occurs at the PA of the dominant polarization mode, has been centered on -45° for display purposes.

a mode transition may be longitudinally resolved provided that θ and M vary slowly with pulse longitude, which is likely the case for PSR B2016+28 for reasons cited in § 2.

The PA change with pulse longitude that is described by equation 6 is shown in Figure 6 for different values of θ_o , with M varying linearly with longitude. The change in average PA predicted by the statistical model (Fig. 6) is qualitatively consistent with what is observed in PSR B2016+28 (cf. bottom panel of Fig. 1). Equation 6 and Figure 6 also illustrate the point that a PA transition between purely orthogonal modes will be discontinuous and instantaneous, whereas nonorthogonal modes will produce a smooth or gradual PA transition (Cheng & Ruderman 1979; SCRWB; Michel 1987).

If, as in SCRWB, one were to convert the PA histograms at each pulse longitude (e.g. Fig. 3) to grey-scale histograms and overlay them on the averaged PA data (e.g. Fig. 6), the average angle would be embedded in the pedestal that appears between the peaks in each histogram because the PA resulting from the superposition of NPM is intermediate to the mode PAs (Eq. 6). In overlaying all the histograms on the average data, the individual pedestals combine to form a much broader pedestal that spans a large range in pulse longitude. This broad pedestal is the modal connecting bridge in PSR B2016+28 discovered by SCRWB (see Fig. 31 of SCRWB).

The preceding point is also illustrated in Figure 4 where actual average angles are shown by the dashed vertical lines in each L-PA scatter plot. In each case, the average angle is not precisely aligned with the dominant mode PA ($\psi = -45^\circ$). The difference between the dominant mode PA and the average PA, $\Delta\psi$, is greatest for PSR B2016+28 and PSR B2020+28 where the modes occur with similar frequency and the mode nonorthogonality is significant. This is to be expected from the model because equation 6 predicts that $\Delta\psi$ is large for $M \simeq 1$ and $\theta > 0$.

4. DISCUSSION

The statistical model’s ability to simulate the rich variety of polarization properties observed in pulsar radio emission provides strong support for the model’s underlying assumption of superposed polarization modes. Observations of PSR B2020+28 support the model’s prediction that the emission will be depolarized on all timescales and that the modes will occur with nearly equal frequency when the polarized intensities of the orthogonal modes are comparable (MS1; MS2). Additionally, the model adequately reproduces observed histograms of total intensity, linear polarization, fractional linear polarization, and PA in PSR B2020+28 (MS1; MS2). Since the polarization modes are superposed and elliptically polar-

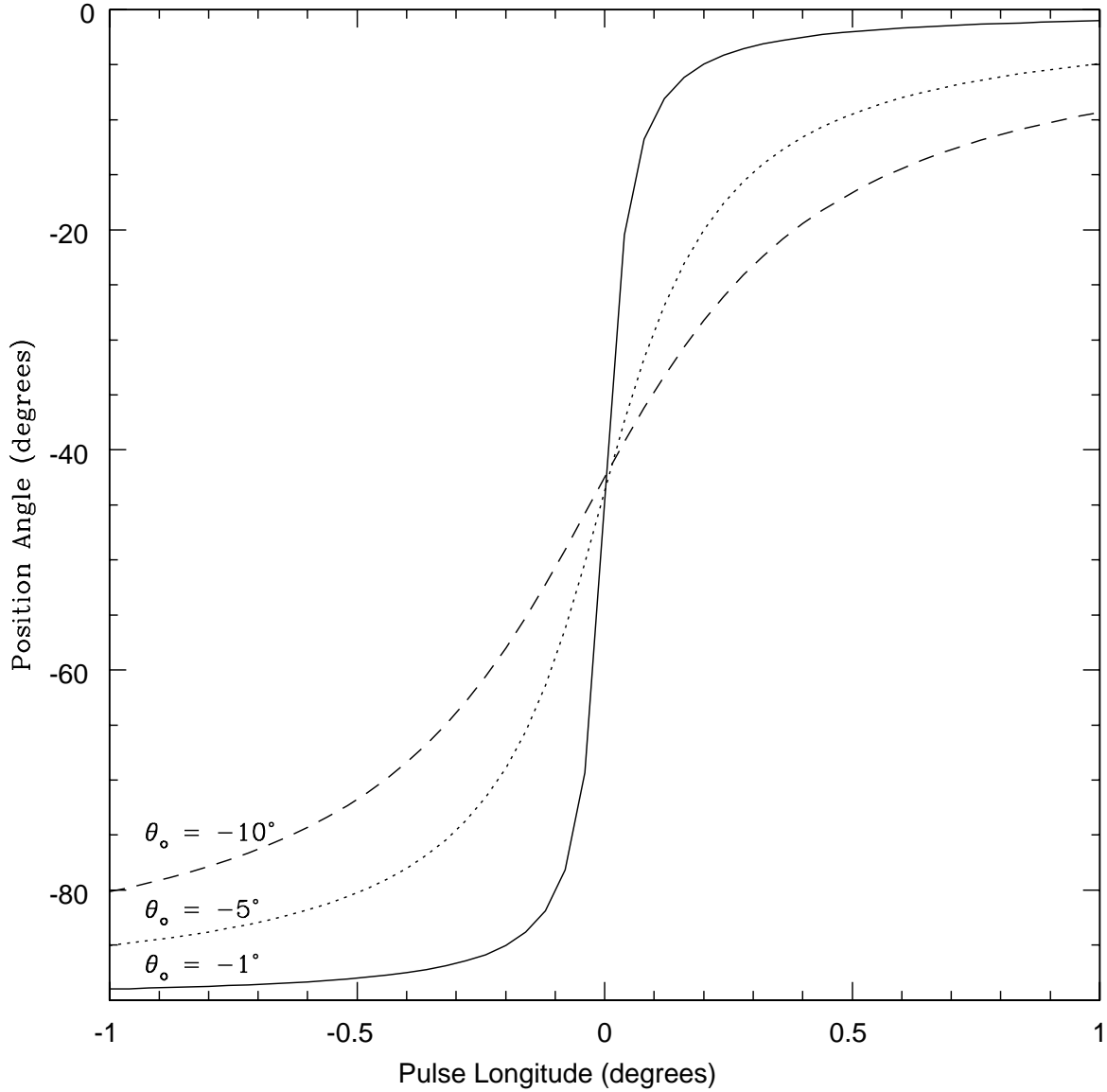


Fig. 6.— Three examples of longitudinally-resolved position angle transitions due to the superposition of nonorthogonal polarization modes. The transitions are more abrupt when the deviation from mode orthogonality, θ_o , is small.

ized in general, the model also predicts that histograms of fractional circular polarization should be unimodal, in accord with the observations (McKinnon 2002). If the modes occurred separately, the histograms of fractional circular polarization would be bimodal, which is not observed. In this paper, the model resolves the longstanding dilemma over the interpretation of the 1404-MHz PAs in PSR B2016+28, accounts for its modal connecting bridge, and explains many subtle features of PA histograms by incorporating the nonorthogonality of the modes.

Obvious questions that arise from an investigation of NPM are: “what is their origin” and “how does the statistical model comport with the explanation of NPM generation”? The task of explaining the origin of OPM is daunting enough by itself, and little attention has been devoted to NPM’s origin because it has been regarded as a minor or subtle aspect of OPM generation. OPM may be intrinsic to the emission mechanism (e.g. Gangadhara 1997; Cheng & Ruderman 1979) or produced at widely separated regions which happen to have magnetic field structure that is orthogonal when projected on the plane of the sky (MTH; Michel 1987). However, the most widely accepted explanation for OPM appeals to propagation effects in the magnetized plasma above the pulsar polar cap (e.g. Allen & Melrose 1982; Barnard & Arons 1986). The radio emission can be spatially separated into two modes of orthogonal polarization due to the difference in their indices of refraction. If the refraction is strong, the emission in one mode that is generated at one location within the magnetosphere may overlap the emission from the other mode that is generated at a different location. In this particular scenario which is entirely consistent with SCRWB’s suggestion that NPM arise from OPM migration, the polarizations of the overlapping modes are not orthogonal because the modes were not generated at the same location. The observed polarization resulting from the overlap of the two nonorthogonal modes is precisely what is illustrated in Figure 2 and described by equations 4 and 5. Therefore, the statistical model is consistent with the proposition that OPM and NPM arise from propagation effects in the pulsar magnetosphere. More generally, the model is consistent with any mode production mechanism that involves the incoherent superposition of the modes. The exact details of how OPM migration actually occurs in PSR B2016+28 are unknown, but may be related to the pulsar’s drifting subpulses (Drake & Craft 1968; Backer 1973) and the occurrence of OPM within them, as in other conal single pulsars such as PSR B0943+10 (Deshpande & Rankin 2001) and PSR B0809+74 (Ramachandran et al. 2002).

In an admirable first attempt to explain NPM, SCRWB modeled the emission’s polarization as the sum of a nonmodal component and OPM. While SCRWB’s model cannot be ruled out, it introduces an additional level of complexity for radiative processes in pulsar magnetospheres by requiring the generation of both a nonmodal emission component and OPM. The statistical model, by contrast, portrays a much simpler situation where radiative

processes are only required to produce two polarization modes, either at emission or through propagation, with slightly nonorthogonal polarizations. Furthermore, the model leads to a simple explanation for the modal connecting bridge in PSR B2016+28. Any other explanation for the bridge would likely resort to rather *ad hoc* assumptions about its origin, placing additional demands on theoretical explanations of radiative processes in the magnetosphere as a result.

A number of observations have posed serious challenges to the validity of the RC model, but the model has generally withstood the test of the observations. The polarization observations of the drifting subpulses in PSR B0809+74 by Taylor et al. (1971) indicated that PA variations were synchronized with the subpulses, and not fixed to the rotation of the star as the RC model predicted. Only recently have Ramachandran et al. (2002) shown that the PA variations within the subpulses are due to OPM transitions, and that the individual modes follow PA trajectories that are consistent with the RC model. Initial observations of OPM (e.g. MTH) also challenged the RC model because it could not account for the production of the modes. However, BRC noted from their single pulse, polarization observations of PSR B2016+28 that the RC model was relevant because the modal PA traces followed parallel trajectories that were consistent with the model. SCRWB pointed out that the 1404-MHz PAs of PSR B2016+28 could be interpreted in the context of the RC model with two, very different viewing geometries. In this paper, the PA interpretation dilemma is resolved and the RC model is thus preserved by accounting for the nonorthogonality of the pulsar’s polarization modes.

The occurrence of NPM has important implications for the interpretation of pulsar polarization and viewing geometry. As shown in SCRWB and this paper, the occurrence of NPM in PSR B2016+28 so disrupts the PA sweep that two, very different interpretations can be made of its viewing geometry. Everett & Weisberg (2001) used some of the most sensitive polarization observations recorded to date in an attempt to tightly constrain the viewing geometry of a number of nearby pulsars. Interestingly, the best fits of their data to the RC model were obtained by completely discarding data recorded on the pulse and relying on data of lower S/N recorded off the pulse. The viewing geometries they determined for PSR B0950+08 and PSR B1929+10 were very different from results obtained in previous work. The fact that both pulsars exhibit NPM (Fig. 5; BR; SCRWB) may explain why data recorded on their pulses deviated significantly from the RC model. Deviations from the RC model have traditionally been attributed to multi-polar magnetic field structure, implying that the emission region is close to the stellar surface. But if the deviations from the RC model are caused by NPM, as suggested here, the emission may originate at a higher location in the magnetosphere where the star’s dipole component dominates the multi-pole components of its magnetic field. Considering the substantial impact of NPM on the

PA sweep in PSR B2016+28, propagation effects may also play a more significant role in determining the observed polarization than other mechanisms, such as relativistic aberration (Blaskiewicz, Cordes, & Wasserman 1991) and current flow above the polar cap (Hibschman & Arons 2001).

In summary, I have incorporated the nonorthogonality of the polarization modes in a statistical model of the polarization of pulsar radio emission. I used the model to show that the rapid change in average PA near the pulse center of PSR B2016+28 at 1404 MHz may be a longitudinally-resolved transition between modes of nonorthogonal polarization, and argued that the PA trajectories of the polarization modes reflect the true viewing geometry of the pulsar. This interpretation preserves the RC model and avoids the unnecessary and unpalatable complication of invoking an additional radiation emission mechanism to explain the pulsar’s modal connecting bridge. The occurrence of NPM in other pulsars is bound to cause their PA sweeps to deviate from the RC model, and although largely ignored in the past, NPM should be taken into account when determining pulsar viewing geometries in future work. The continuing ability of the statistical model to simulate the rich variety in the observed polarization properties of pulsars lends support to the model’s applicability and its fundamental, underlying assumption that the polarization modes occur simultaneously.

I thank Dan Stinebring for providing the data used in this analysis, and Joanna Rankin for constructive comments on the manuscript. The Arecibo Observatory is operated by Cornell University under cooperative agreement with the National Science Foundation.

REFERENCES

- Allen, M. C. & Melrose, D. B. 1982, *Proc. Astron. Soc. Aust.*, 4, 365
- Backer, D. C. 1973, *ApJ*, 182, 245
- Backer, D. C. & Rankin, J. M. 1980, *ApJS*, 42, 143 (BR)
- Backer, D. C., Rankin, J. M., & Campbell, D. B. 1976, *Nature*, 263, 202 (BRC)
- Barnard, J. J. & Arons, J. 1986, *ApJ*, 302, 138
- Blaskiewicz, M., Cordes, J. M., & Wasserman, I. 1991, *ApJ*, 370, 643
- Cheng, A. F. & Ruderman, M. A. 1979, *ApJ*, 229, 348
- Cordes, J. M., Rankin, J. M., & Backer, D. C. 1978, *ApJ*, 223, 961
- Deshpande, A. A. & Rankin, J. M. 2001, *MNRAS*, 322, 438
- Drake, F. D. & Craft, H. D. 1968, *Nature*, 220, 231
- Everett, J. E. & Weisberg, J. M. 2001, *ApJ*, 553, 341
- Gangadhara, R. T. 1997, *A&A*, 327, 155
- Hankins, T. H. & Rickett, B. J. 1986, *ApJ*, 311, 684
- Hankins, T. H., Rankin, J. M., Stinebring, D. R., & McKinnon, M. M. 1992, in *Proceedings of IAU Coll 128, The Magnetospheric Structure and Emission Mechanisms of Radio Pulsars*, ed. T. Hankins, J. Rankin, & J. Gil, (Zielona Góra: Pedagogical University Press), 161
- Hibschman, J. A. & Arons, J. 2001, *ApJ*, 546, 382
- Manchester, R. N., Taylor, J. H., & Huguenin, G. R. 1975, *ApJ*, 196, 83 (MTH)
- Mardia, K. V. 1972, *Statistics of Directional Data*, (London: Academic), 24
- McKinnon, M. M. 2002, *ApJ*, 568, 302
- McKinnon, M. M. & Stinebring, D. R. 1998, *ApJ*, 502, 883 (MS1)
- McKinnon, M. M. & Stinebring, D. R. 2000, *ApJ*, 529, 435 (MS2)
- Michel, F. C. 1987, *ApJ*, 322, 822
- Radhakrishnan, V. & Cooke, D. J. 1969, *Astrophys. Lett.*, 3, 225 (RC)
- Ramachandran, R., Rankin, J. M., Stappers, B. W., Kouwenhoven, M. L. A., & van Leeuwen, A. G. J. 2002, *A&A*, 381, 993
- Rankin, J. M. 1983, *ApJ*, 274, 333
- Rankin, J. M. 1986, *ApJ*, 301, 901

Rankin, J. M. 1993, *ApJS*, 85, 145

Rankin, J. M. & Ramachandran, R. 2003, *ApJ*, in press

Stinebring, D. R., Cordes, J. M., Rankin, J. M., Weisberg, J. M., & Boriakoff, V. 1984, *ApJS*, 55, 247 (SCRWB)

Taylor, J. H., Huguenin, G. R., Hirsch, R. M., & Manchester, R. N. 1971, *Astrophys. Lett.*, 9, 205